Application of Acoustic Techniques to Fluid-Particle Systems – A Review

Fria Hossein*, Massimiliano Materazzi, Paola Lettieri, Panagiota Angeli

Department of Chemical Engineering, University College London, London, WC1E 7JE, United Kingdom. *f.hossein@ucl.ac.uk

Abstract

Acoustic methods applied to opaque systems have attracted the attention of researchers in fluid mechanics. In particular, owing to their ability to characterise in real-time, non-transparent and highly concentrated fluid-particle systems, they have been applied to the study of complex multiphase flows such as fluidised beds. This paper gives an overview of the physical principles and typical challenges of ultrasound and acoustic emission AE methods when applied to fluid-particle systems. The principles of ultrasound imaging are explained first. The measurement techniques and signal processing methodologies for obtaining velocity profiles, size distribution of the dispersed phases, and solid volume fraction are then discussed. The techniques are based on the measurement of attenuation, sound speed, frequency shift, and transit time of the propagated sound wave. A description of the acoustic emission technique and applications to fluid-particle systems are then discussed. Finally, extensions and future opportunities of the acoustic techniques are presented.

1. Introduction

The flow of multiphase mixtures is complex and involves a wide range of length and time scales. The development of predictive models for such systems is dependent on the availability of experimental data on the spatial and temporal distribution of the phases and on their velocities. The experimental study of dispersed patterns in particular, including solid particle flows and gas-liquid or liquid-liquid dispersions, is demanding as it involves the presence of many interfaces and a wide size distribution of the suspended phase. Particle-fluid flows appear in fluidisation, pneumatic conveying, and solids processing, with applications in nuclear power generation and in wastewater treatment (Klinzing et al., (2011), Wang et al., (2019), Werther, (1992), Yates and Lettieri, (2016)). Dispersed liquid-liquid or gas-liquid flows are common in two-phase separations and reactions, with applications in extraction of metals or pharmaceuticals, in bubble columns for treating wastewater and in the transport of multiphase mixtures in the oil and gas industries (Ngan et al., (2009)). Despite extensive research studies in this area, the structure of dispersed flows, especially at high dispersed phase fractions and in

unsteady-state conditions, is not entirely understood (Poelma et al., (2006), Voulgaropoulos and Angeli, (2017))

Many measurement techniques have been developed in order to understand the physical phenomena underpinning multiphase flows, and these are classified as *invasive* and *non-invasive*. Examples of invasive measurement techniques are impedance and optical fibre probes (Serizawa et al., (1991), Muñoz-Cobo et al., (2017)). The principles of these techniques are based on the differences in the various phases of the electrical properties for impedance probes (Spinelli et al., (2019)) and of the light transmission properties for fibre optical probes. Other examples of invasive techniques are hot wire or hot film anemometers and thermocouples, which also disturb the flow field and can thus affect the accuracy of the measurements (Bohs et al., (2000), Farage et al., (1997)).

The non-invasive measurement techniques are classified by their working principle, and include electrostatic, acoustic, positron emission particle tracking (PEPT), X-ray imaging (Wang et al., (2019)), laser Doppler anemometry (LDA), optical particle image velocimetry (PIV), magnetic resonance imaging (MRI) (Pore et al., (2015), Boyd and Varley, (2001)), and tomography methods such as ECT (electrical capacitance tomography) (Li et al., (2018)), and EMT (electromagnetic tomography) (Han-liang and Ling-an, (2000)). The optical techniques (e.g., PIV and LDA) are suitable for highly diluted dispersed systems with volume fractions lower than 5% (Patricia and Derek, (2000), Poelma, (2017)). These techniques require optically transparent test sections; to increase the range of volume fractions that can be studied, the refractive indexes of the phases should be matched so that the system remains transparent. (Poelma, (2020), Su et al., (2007)). Refractive index matching limits the range of liquids and solids that can be studied, which are not always representative of industrial applications. MRI techniques are expensive and require complex signal processing methodologies (Boussel et al., (2009)). X-ray imaging is a penetrating form of high electromagnetic radiation (Halls et al., (2018), Chirone et al., (2018)) and has been applied to gas-solid or gas-liquid systems only, e.g., systems with significant differences in phase densities and radiation transparency. Tomography methods e.g., ECT have been successfully applied to the study of two-phase flow phenomena in fluid-particle flows; the ECT technique measures the electrical capacitances between sets of electrodes, placed around the fluidised beds. The sensors in EMT are made of a set of excitation coils to produce a magnetic field within a pipe cross section and of a set of detection coils to detect the changes in the field due to changes in permeability and conductivity inside the pipe or vessel (Ismail et al., (2005)). An overview of non-invasive and invasive measurement techniques for fluid-particle flows is given in Table 1.

Table 1 : An overview of measurements techniques in fluid-particle flows

Techniques	**What can be measured?**	**Pros**	**Cons**	**References**
Fibre optic probes (invasive)	Void fraction, local flow velocity and characteristic size.	Electromagnetic interference immunity, high temperature applications, high resolution	Tracer material relatively expensive, end-user unfamiliarity	(Rojas and Loewen, (2007), Maaß et al., (2011), Poelma, (2020))
Hot film anemometry (invasive)	Void fraction and slip velocity	Cheap, high temporal resolution,	Heat transfer and aerodynamic problems	(Wang and Ching, (2001), Örlü and Alfredsson, (2010))
Thermocouples (invasive)	Fluid temperature	Simple, inexpensive, large variety temperature	Reference is less stable	((2008))
Positron emission particle tracking (non-invasive)	Tracking a single particle, mapping the concentration	Relatively open channel geometry, high temporal resolution	Radioactive tracer particles are used	(Parker and Fan, (2008), Windows-Yule et al., (2020))
Optical particle image velocimetry (PIV) (non-invasive)	Velocity of dispersed phase	Superior time resolution, qualitative flow field mapping	Small penetration depth, requires dilute systems	(Yang and Johnson, (2017), Yee et al., (2019))
Electrical capacitance tomography ECT (non-invasive)	2D/3D Volume fraction and phase distribution	Relatively cheap and fast	Low resolution(>>1 mm)	(Flores et al., (2006), Lei and Liu, (2011))
Ultrasound	Volume fraction, velocity profiles, particle size distribution	Relatively cheap, temporal resolution high	Only suitable for liquid as continue phase	(Hunter et al., (2011), Hossein, (2019))
MRI (non-invasive)	Volume fraction, average velocity.	Can measure despite presence of gas, low time resolution	Expensive, material restrictions, slow, high safety hazardous	(Gladden, (2003), Ramskill et al., (2018))
X-Ray (non-invasive)	Phase distribution 2D or 3D	No limitation on materials. High resolution	Expensive, high safety hazardous	(Macrì et al., (2020))

Ultrasound techniques offer the possibility of non-intrusive, low-cost measurements, which can be used in non-transparent test sections (Laurent et al., (2001), Afaneh et al., (2011), Allegra

and Hawley, (1972)). They have been applied in areas such as medical imaging of gallstones (De-la-Cruz-Torres et al., (2020), Ortiz et al., (2012)), ionic fluid imaging in animal tissue (Hossein and Wang, (2019)), measurement of atomic weight and ionic charges of colloidal suspensions (Hossein and Wang, (2020)), measurement of the physicochemical properties of nanoparticles including shape and charge in colloids (Hossein, (2019)). The time of flight (TOF)-based technique has been used to detect ice particles in slurry flow (Sari et al., (2000)), while the Doppler method has been used to obtain velocity profiles in oil-water stratified flows (Xiaoxiao et al., (2015), Weiling et al., (2018)). Ultrasound techniques have been applied to the measurement of porosity and compressibility of suspended particles (Han et al., (2017)), particle size distribution (PSD) (Wöckel et al., (2012), Tsujimoto et al., (1999), Tran et al., (2016)), particle and bubble velocity profiles and porosity in porous materials (Zhou et al., (2013), Wang et al., (2002), Hunter et al., (2011)). Acoustic emission AE technique has been applied to the measurement of particle size and bed height in solid-gas fluidised bed (Tsujimoto et al., (1999)). The use of acoustic emission AE signal to establish the particle size distribution in solid-gas flows was reported by (Uher and Beneš, (2012)). Medwin, (1976) used ultrasound to study the behaviour of a single bubble suspended in a liquid phase and determine the effect of bubble size on resonance frequency. Cents et al., (2004) developed a technique to measure the size distributions and phase holdup of particles, droplets, and bubbles in two-phase, and three-phase systems. They showed that the technique was able to resolve the size distribution of solid particles in the presence of gas bubbles. Jingyuan and Yong, (2016) measured with ultrasound the particle size in a solid-gas fluidised bed system. Povolny et al., (2018) with a pulse-echo technique obtained the horizontal position of rising air bubbles in a water tank and showed that multiple bubbles could be detected concurrently. Wongsaroj et al., (2018) obtained instantaneous velocity profiles of the liquid phase and the bubbles separately in the bubbly flows based on the Doppler Effect using a single resonant frequency transducer. An extensive review on ultrasound image velocimetry techniques and their challenges was given by (Poelma, (2017)). The review focused on the application of cross correlation techniques to estimate velocities (echo PIV) from ultrasound-based image.

Different ultrasound methods e.g., transit time, Doppler effect, and attenuation spectroscopy can be used to characterise dispersed phases in liquid-solid, liquid-liquid, and liquid-gas flows. Ultrasound propagation speed and attenuation depends on the properties of the medium such as density and compressibility; these methods can therefore be used to measure the volume fraction of the dispersed phase in fluid-particle flows (Han et al., (2017), De-la-Cruz-Torres et al., (2020)). Ultrasound can also be used to measure the particle velocity profiles in liquid-solid flows (Doppler Effect) and to characterize particle size distribution based on attenuation spectroscopy approaches (Wongsaroj et al., (2018), Nan et al., (2019)). This technique works

well for low and high volume fractions of the dispersed particles, but due to high attenuation of ultrasound in air, it cannot be used to monitor particles in particle-gas flows. The acoustic emission technique (AE) can be used in solid-gas flows. In such gas-solid systems, elastic waves are generated from the particle-particle or particle chamber wall collisions or friction (Atkinson and Kyto¨maa, (1993)). The sound generated by the friction, collisions and fluid turbulence in gas-particle systems includes not only audible sound, detectable by a microphone, but also high frequency sound in the non-audible range (Xu et al., (2021)). The generated elastic waves (or sound) can be recorded by a microphone or an acoustic emission (AE) sensor. Particles in solid-gas flows can be monitored and characterized once the correlation between particular elastic waves and particle motion is established (Tsujimoto et al., (1999)). The AE technique can also be applied to other systems such as liquid-particle flows.

The main drawbacks of the ultrasound techniques are the relatively low resolution and the maximum achievable frame rate (Poelma, (2020)). The use of high ultrasound frequencies can improve the resolution, but it leads to high signal attenuation or reduced penetration depth (Ortiz et al., (2012)). In addition, ultrasound techniques are only suitable when the continuous phase is liquid. AE techniques, on the other hand, suffer from low amplitude (acoustic signal is usually weak and operating environments are often noisy which make the discrimination of the signal very difficult), disturbances from high frequency signal sources such as turbulence, or interference from nearby electromagnetic sources.

In this paper, we review advances on the application of ultrasound-based and acoustic emission AE techniques to the study of fluid-particle systems. The basic principles of ultrasound imaging have previously been reviewed (Wu et al., (2020), Yan et al., (2020), Zhang et al., (2020)). However, the signal processing approaches for obtaining velocity profiles, dispersed phase size distribution and volume fraction have not been systematically presented. The use of different sensors for various applications is an essential part of the measurement technique but has not been discussed extensively in the existing literature. We review the ultrasound techniques and their signal processing for online measurements in fluid-particle systems. The measurement methods based on transit time and attenuation are discussed in Section 2. Section 3 describes the signal processing approaches for obtaining velocity profiles, particle size and volume fraction. The acoustic emission AE technique for measurements in particle-gas flows is discussed in Section 4. Section 5 summarises the conclusions and discusses opportunities for further improvements and applications.

2. Basic Principles of Ultrasound Techniques

In ultrasound based techniques, a high-frequency sound wave (typically 1–20 MHz) is passed through the flow area of interest using a probe (transducer) (Wells, (1975)). The choice of frequency can affect the resolution of the image or the depth of the area that can be investigated. A low frequency signal gives a lower quality image but can penetrate deeper into the medium, whereas a high frequency improves the image resolution at the cost of high attenuation and shallow penetration (Pirri et al., (2020), DosRamos, (2012)). In ultrasound imaging, the main concern is the attenuation of the propagated sound wave in the medium, which causes a reduction in signal amplitude. Here, we are briefly describing the time-of-flight TOF and attenuation of ultrasound as an important parameter for the fluid-particle system characterizations. In fluid-particle system TOF and attenuation of sound wave are proportional to the volume fraction of the particles, and they can be used as a tool to characterize the volume fraction of the mixture.

2.1 Time of Flight (TOF)

When an ultrasound wave propagates through a fluid-particle system, it is partially reflected by the particle interfaces due to the difference in acoustic impedance between the fluid and the particles. The wave is reflected back and detected by the same transducer. The transducer records the time taken for the transmitted wave to be reflected back from the interface, which is called the Time of Flight (TOF) (Atkinson and Kyto¨maa, (1993)) and is given by:

$$x = \frac{1}{2} t \times c \qquad (1)$$

where x is the distance, c is the ultrasound velocity in the medium, and t is the TOF through the medium. The factor ½ is introduced because the signal travels twice through the medium, to the particle and back. In some cases, the reflection of sound is minimal due to the similarities in the acoustic impedance of the materials (Hossein, (2019), Baker, (2005)).

2.2 Attenuation

Attenuation of the sound wave can be caused by several factors such as absorption, scattering, reflection, divergence, and diffraction. *Absorption* is the reduction of intensity which happens when the ultrasound propagates through a medium and some of its energy is lost in the form of heat. *Scattering* occurs when the ultrasound wave strikes a different medium. *Reflection* occurs when the ultrasound wave travels from one medium to another that has different impedance

(Wu et al., (2020)). *Divergence* is the spreading of the sound wave beyond the focal point of the probe. *Diffraction* happens when the wave passes around a barrier. The presence of particles in fluid-particle systems, attenuates the sound wave; the attenuation is increased with the particle concentration (Stakutis et al., (1955)). This is due to the impedance difference between the solid particles and the fluid (Soong et al., (1997)). The attenuation coefficient of sound(α_s) wave transmitted through a medium over length x can be calculated by:

$$A_i = A_o e^{-\alpha_s x} \tag{2}$$

where A_i is the attenuated amplitude and A_o is the initial amplitude of the sound wave. The acoustic impedance, Z describes the resistance to an ultrasound beam as it passes through a medium and is given by $Z = \rho . c$ where ρ and c are the medium density and the ultrasound speed in that medium, respectively. When an ultrasound wave encounters an interface between two media with different acoustic impedances, Z_1 and Z_2, part of it is transmitted and part of it is reflected. If the incident wave has amplitude A_i and approaches the interface with angle θ_i, the reflected wave has amplitude A_r and angle θ_r, and the transmitted wave has an amplitude A_t and angle θ_t, then Snell's law (Savino and Ambrosio, (2019)) can be applied:

$$\frac{sin(\theta_i)}{c_1} = \frac{sin(\theta_t)}{c_2} = \frac{sin(\theta_r)}{c_1} \tag{3}$$

The reflection coefficient, *R*, is then given by:

$$R = \frac{Z_2 cos(\theta_i) - Z_1 cos(\theta_t)}{Z_2 cos(\theta_i) + Z_1 cos(\theta_t)} \tag{4}$$

3. Application of Ultrasound to Fluid-Particle Systems

In fluid-particle system is of interest to measure several different parameters of these opaque system, e.g., velocity profiles, particle size, and volume fractions. There are currently no single techniques available to that able to measure all these parameters, therefore ultrasound technique can be introduced to measure all these parameters. In this section, the ultrasound signal processing methodology for obtaining important parameters in fluid-particle flows is discussed, including average velocity and velocity profiles of both continuous and dispersed phases (Section 3.1), dispersed phase size distribution (Section 3.2) and volume fraction of the particles (Section 3.3).

3.1 Velocity Profile Measurements

The transit time method can be used for measuring the velocity of a single-phase liquid (e.g., water), and the Doppler shift technique used for measuring the velocity profile of particles in fluid-particle flows are described below.

Transit Time Method: In this method, the propagation time of the ultrasound signal is measured between the emitting and the receiving transducers. The principle of this technique is shown in Figure 1, where the first transducer is mounted at the top of the pipe with angle of inclination θ and the second transducer is mounted at the bottom of the pipe with the same inclination angle. This technique has been widely used to obtain average velocity in single-phase flows (Thi et al., (2020), Nguyen and Park, (2019)).

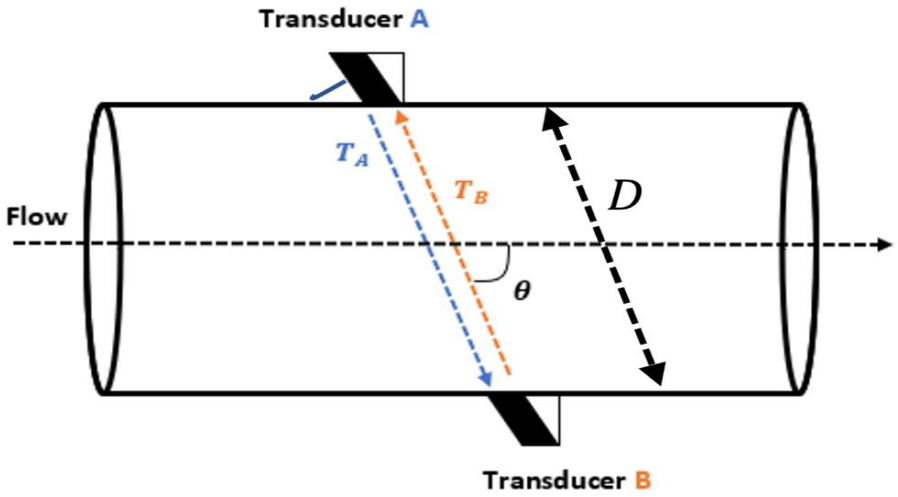

Figure 1: Transit time average velocity measurement geometry.

The propagation of a sound wave in a fluid can be described as a vibrating motion where molecules or atoms are displaced from their normal positions**,** which means that if the fluid is moving, then the sound wave will move with the fluid (Conrad and Lynnworth, (2002))**.** In Figure 1 with the flow moving from left to right, if the wave is propagating from Transducer B across the pipe towards Transducer A, the wave propagation speed will slow down, whereas if the ultrasound wave propagates from Transducer A to Transducer B the wave propagation speed will increase (Raine et al., (2015)). The propagation time, T_A, of the wave from Transducer A to Transducer B is given by:

$$T_A = \frac{D}{c + v\cos\theta} \tag{5}$$

where θ is the angle between the flow and the wave propagation direction, and D is the distance between Transducers A and B. When the ultrasound propagates upstream from Transducer B to Transducer A the propagation time, T_B, is given by:

$$T_B = \frac{D}{c - v\cos\theta} \tag{6}$$

From Equations 5 and 6, the average flow velocity, v, can be found as follows:

$$v = \frac{(T_B - T_A)\, c^2}{2\, D\cos\theta} \tag{7}$$

The transit time method works well for single-phase flows and is widely used in practice to measure the velocity of gases or liquids within industrial applications (Eren, (1998), Mori et al., (2002)). The technique encounters problems in dispersed multiphase flows due to the scattering of the sound wave by the suspended particles or drops/bubbles. As a result, the wave can be significantly attenuated and may not be recorded by the receiving transducer (Vatanakul et al., (2004), DosRamos, (2012)).

Doppler Method: The Doppler Effect is a change in the frequency of the sound wave when it impacts objects that have different velocity to the sound source. To measure velocity with the Doppler method in a flowing fluid, tracers (such as bubbles or particles) are added, which shift the frequency of the sound wave (Takeda, (1986)). The frequency shift is predicted by the Doppler theory. This method is widely used in medicine (Chun et al., (2011), Sigel, (1998)); in multiphase flows it has been used to measure the velocity profiles of solid particles in dispersed solid-liquid flows (Meribout et al., (2020), Tomonori et al., (2013), Takeda. Y., (2013)) and bubble velocity profiles in bubbly flows (Aritomi et al., (2000)). Earlier research has shown that the Doppler shift is proportional to the phase velocities (Thong-un et al., (2018)). Velocities of dispersed drops in oil-water flows have also been measured with this approach (Liu et al., (2018)).

A schematic set-up for measuring the velocity of solids in solid-fluid flows based on the Doppler Effect together with the signal processing approach is shown in Figure 2.

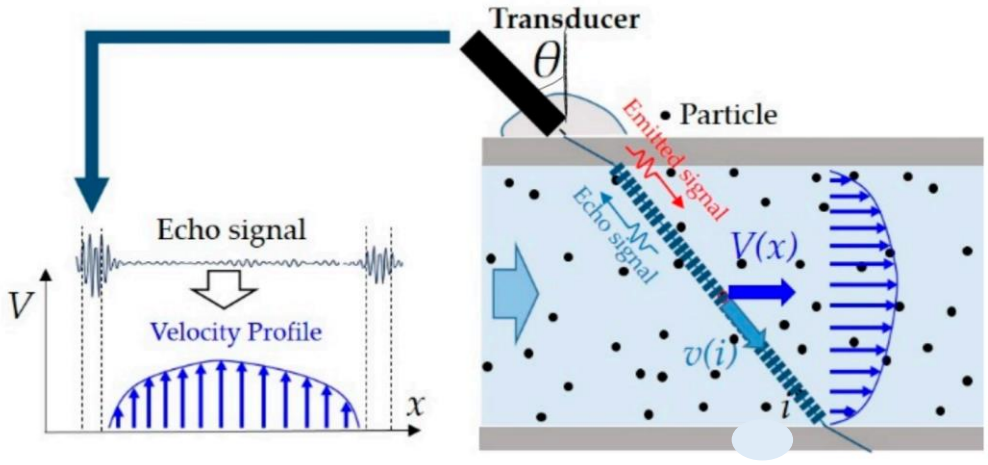

Figure 2: Ultrasound Doppler velocity profile measurement configuration and geometry, echo signal and velocity profile configurations (Wongsaroj et al., (2018)).

An ultrasound wave is transmitted into the flow by the transducer, and the reflected (backscattered echoes) signal is recorded by the same transducer. To measure the velocity profile along the wave path x, the procedure is repeated after a short time (of the order of microseconds), and the two signals are cross-correlated (Card et al., (1971)). The velocity profile along the ultrasound wave path can be calculated using Equation 8:

$$V(x) = \frac{c}{2f_o \sin\theta} f_d(x) \tag{8}$$

where f_o is the transmitted frequency, f_d is the Doppler frequency, c is the sound speed in the medium and θ is the incident angle (Wongsaroj et al., (2018)). The reflected (echo) signal,$e(t)$, received by the same transducer theoretically can be expressed as:

$$e(t) = Acos2\pi(f_o(t - t_n) + n\left(\frac{f_d(x)}{f_{prf}}\right) \tag{9}$$

where t_n represents the delay time of the reflected signal at n (number of pulses), A is the signal amplitude of the reflected signal and f_{prf} is the pulse repetition frequency. To obtain the velocity profile from Equation 8, the Doppler frequency from Equation 9 is required. The Doppler signal is extracted from the reflected signal, $e(t)$, and is estimated using FFT (Fast Fourier Transform) from the following equations (Thong-un et al., 2018). Firstly, the echo signal $e(t)$ is treated with a low pass filter (noise removed) to eliminate the carrier wave component in Eq 10, and then the magnitude of each frequency bin is calculated by Eq 11. The subscripts I and Q in Eq 10 refer to the sine and cosine terms

$$[2e(t)exp(i2\pi f_o t)]_{low\ pass\ filter} = x_I(t) + ix_Q(t). \quad (10)$$

$$X_{magnitude}(f) = \sqrt{X_I^2(f) + iX_Q^2}(f) \quad (11)$$

where, $X_I(f)$ and $X_Q(f)$ are the DFT (Discrete Frequency Transform) of $x_I(t)$ and $x_Q(t)$. To express the power spectrum, we need to carry out FFT for each reflected pulse.

$$\begin{aligned} P_{forward}(f) &= \left(Re[X_I(f)] - Img[X_Q(f)]\right)^2 + (Re[X_Q(f)] + Img[X_I(f)])^2 \\ P_{backward}(f) &= (Re[X_I(f)] + Img[X_Q(f)])^2 + (Re[X_Q(f)] - Img[X_I(f)])^2 \end{aligned} \quad (12)$$

Where P is the power spectrum, and finally the Doppler frequency can be determined by:

$$f_d(x) = \frac{\sum f(P_{forward}(f) - P_{backward}(f))}{\sum f(P_{forward}(f) + P_{backward}(f))} \quad (13)$$

Finally, the computed $f_d(x)$ is inserted into Equation 8 to calculate the particle velocity profile. When there are many particles in the mixture, the number of pulses, n e.g., the number of reflected pulses from the mixture, could be counted, and similar to a single particle (explained above), the signal processing could be carried out for a large number of particles.

The above technique is the most used method to measure frequency shift, although it is not the most accurate. This is because both the signal transmitted through the mixture, and the signal reflected by the moving particles are received by the same transducer. This leads to an error as the signal travels along the same path for a second time while changing its frequency. Another error arises as the transducer switches from the transmitting to the receiving mode, which can result in loss of some of the signal (Wongsaroj et al., (2018)). A better way to measure the Doppler shift frequency would be to use two transducers, one as a transmitter and the other as a receiver, see Figure 3, with the signal travelling only once through the mixture (Xiaoxiao et al., (2015)).

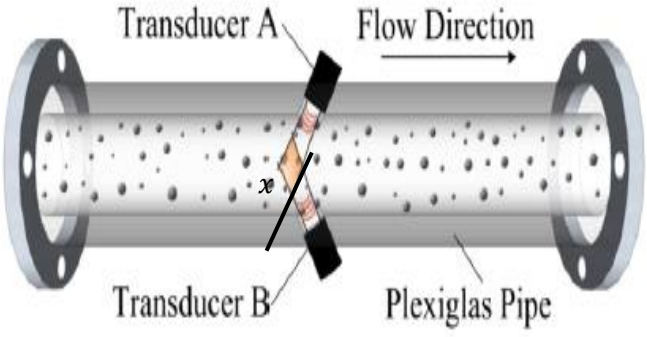

Figure 3: Ultrasound Doppler velocimetry [ultrasound wave propagated along the x-direction] (Xiaoxiao et al., (2015)).

The wave received by a tracer particle will have a frequency, f_1, which is different to the emitted frequency f_o and is given by:

$$f_1 = \frac{c + V(x)\cos\theta}{c} f_o \tag{14}$$

where $V(x)$ denotes the particle velocity, c is the speed of sound in the continuous fluid, and θ denotes the transducer inclination angle. The acoustic wave scattered by the particle that is received by Transducer B has frequency f_r given by:

$$f_r = \frac{c}{c - V(x)\cos\theta} f_1 \tag{15}$$

From Eq 14 and Eq 15 the frequency shift, $f_d(x)$, can be found as:

$$f_d(x) = f_r - f_o = \left[\frac{2V(x)\cos\theta}{c}\right] f_o \tag{16}$$

From Equation 16, the velocity profile of the particles *V(x)* along the direction of the ultrasound wave propagation (Figure 3) can be calculated as:

$$V(x) = \frac{c}{2\cos\theta} \frac{f_d(x)}{f_o} \tag{17}$$

For accurate results using the Doppler method, it is important to know the correct Doppler angle,α, (the angle between the ultrasound wave propagation direction and the flow direction (see Figure 4 a). The following equation can be used to calculate the Doppler angle:

$$\cos\alpha = \frac{c_3}{c_1}\cos\theta \tag{18}$$

where, $c_1$is the sound speed in the ultrasound gel, $c_3$is the sound speed in the fluid-particle flow, α and θ are the Doppler angle and transducer incline angle, respectively. The difference between α and θ can be small if the gel and the continuous fluid in the pipe have similar acoustic impedance and this is the case when the test fluid is water. However, if the test fluid is not water, this difference may be large and cannot be ignored.

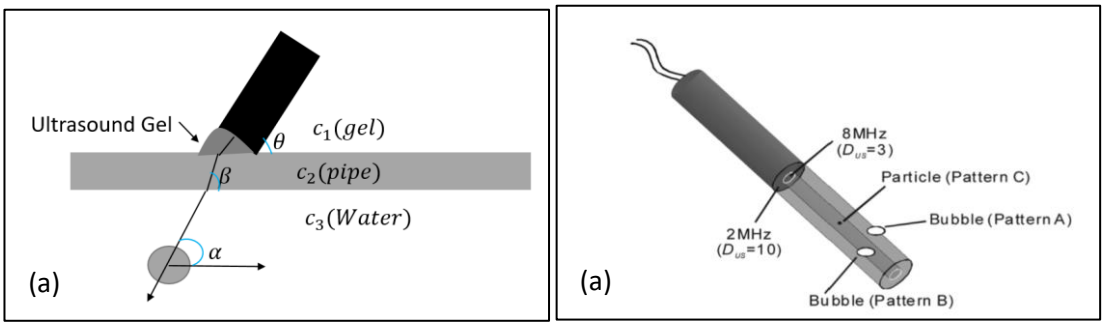

Figure 4: a) Detection of the angle between ultrasound wave propagation direction and flow direction (Wang et al., (2002)), b) schematic diagram of a multi-wave transducer (Kikura et al., (2009)). .

A technique which utilises a multi-element transducer that produces waves with different frequencies has been applied to the simultaneous measurement of both liquid and bubble velocities in dispersed bubble- solid flows (Kikura et al., (2009)). The transducer used had an inner element with 3 mm diameter operating at 8 MHz frequency and an outer element with 10 mm diameter operating at 2 MHz frequency (Figure 4 b) and was installed on the outer surface of the test section with an angle of 45° facing downwards. The signals reflected from the phases were then recorded by the same transducer. The measurements were carried out in a suspension of micro plastic particles used as tracers (at concentration of 0.2 g/L) and of bubbles (2.5 mm) at void fraction of 1.8% . The inner transducer element indicated the liquid velocity using the particles as tracers, while the outer element was used to calculate the bubble rising velocity. The signal processing is more complex in the case of multi-element transducers compared to single element ones. A combination of the reflected signals at 2 MHz and 8 MHZ is shown in Figure 5, where D_{us} denotes the probe element diameter (see Figure 4 b).

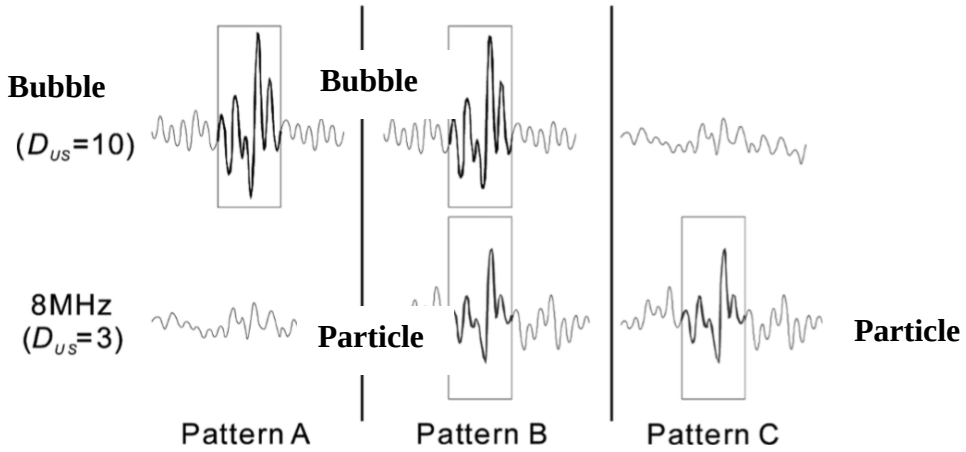

Figure 5: Ultrasound signal patterns (Kikura et al., (2009), Hiroshige et al., (2009)).

As can be seen in Figure 5, in Pattern A, the reflected signal appeared at 2 MHz, from the bubbles, but there is no reflected signal at 8 MHz. In Pattern B, the reflected signals appeared at both the 2 MHz and 8 MHz, including both particles and bubbles. In Pattern C, the signal is reflected only at 8 MHz from the particles. The bubble velocities were obtained using the reflected signals at 2 MHz from Patterns A and B. The liquid velocity profiles were found by subtracting Pattern B from the recorded signals at 8 MHz, and the particle velocities were obtained using the reflected signals at 8 MHz in Pattern C.

3.2 Particle Size Distribution (PSD)

Ultrasound has been used to analyse particle size distribution in multiphase flows for solids concentrations up to 60% (Nan et al., (2019), Patricia and Derek, (2000)) and a wide range of particle sizes, from 10 nm to 1 mm (Thao et al., (2016), Vatanakul et al., (2004)). Two types of waves have been applied: continuous and pulsed longitudinal waves (Atkinson and Wells, (1977)). Pulsed waves are preferred to continuous ones to avoid the effects of acoustic interference (where two waves with similar frequency in a medium combine and produce a constructive or destructive wave (Mingxu et al., (2008)). In the measurements, ultrasound waves with different frequencies are emitted by the transmitter and the attenuated signals are collected by a receiver (Spelt et al., (1999)). The attenuation coefficient can then be calculated using Equation 2 (Riebel and Loffler, (1989)). An example of the relationship between particle size and attenuation spectrum for different frequencies is shown in Figure 6.

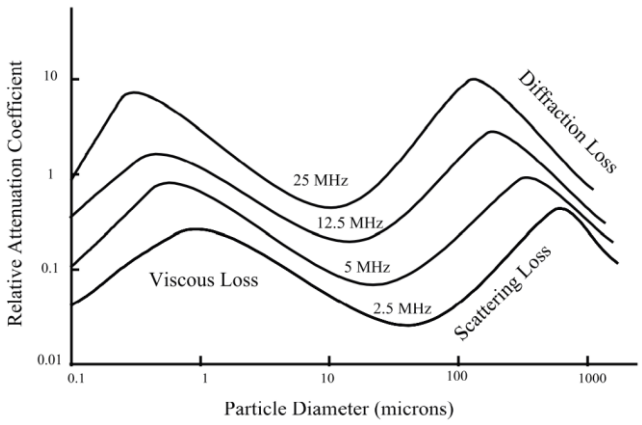

Figure 6: Variation of relative attenuation coefficient with particle size at different frequencies (Mougina et al., (2003)).

From Figure 6 it is clear that if attenuation is measured at a single frequency, only four mono-size populations (two in the region of viscous attenuation, one in the scattering loss region and the fourth in the diffraction zone) could be produced. This is the reason that a range of frequencies is used. To obtain the particle size distribution (PSD), the attenuation of the ultrasound signal propagating through a fluid-particle flow is measured as a function of frequency. The FFT method can be used to obtain the broadband ultrasonic spectrum, from which the attenuation spectrum is calculated for each frequency. In most cases, the PSD is derived from the acoustic attenuation measurements by using the Epstein and Carhart (Epstein and Carhart, (1953)) and Allegra and Hawley (Allegra and Hawley, (1972)) (ECAH) model. The model considers the scattering of the ultrasound by a single particle and relates the attenuation spectrum with the physical properties of the particle. The physical properties of each phase are required, including sound velocity, density, thermal expansion coefficient, heat capacity, thermal conductivity, viscosity of continuous phase, and shear rigidity of the solid sphere. In the ECAH model the attenuation is related to the physical properties as follows:

$$\alpha = \alpha(f, \emptyset, r, P) \tag{19}$$

where α denotes the attenuation spectrum vector, and r is the particle radius. Theoretically, the attenuation is a function of frequency f, particle volume fraction φ_r, particle radius r and a physical vector P which contains all physical properties. The ultrasound attenuation, α, in the fluid-particle system is taken as the sum of scattering effects from each particle, and is expressed as:

$$\alpha = \frac{3\varphi_r}{k^2} . \sum_{j=1}^{N} \frac{1}{(r_j)^3} . \sum_{n=0}^{\infty} (2n+1)[A_n(r_j, \omega_i)] \qquad (20)$$

where $k = \frac{2\pi}{\omega}$, is the wavenumber of the emitted wave, $A_n$is the scattering coefficient, which is a function of (kr), k and r are the wave number and the particle radius respectively, and N is the number of points in the attenuation spectrum. The integer $(n = 0,1,2,3 \ldots)$ corresponds to the nth partial wave and represents different angular modes (monopole n = 0, dipole n = 1, quadrupole n = 2, and so on). The variation of the scattering coefficient An plays a key role in the calculation of the attenuation coefficient. The attenuation caused by the particles having diameter $2r$ and volume fraction φ_r is proportional to $\frac{\varphi_r}{8r^3}$, (Riebel and Loffler, (1989)), and the attenuation coefficient can be calculated as follows. The inversion process to solve the form of matrix of Equation 20 is expressed by (Jia et al (2019)) as:

$$\alpha(\omega_i) = \frac{3\varphi_r}{2} \int \frac{1}{k^2(r_j)^3} \sum\nolimits_{n=0}^{\infty} (2n+1)\left[A_n((r_j, \omega_i)\right] dr \sum V \Delta r_i \qquad (21)$$

G_i A_{ij} F_i

$$AF = G \qquad (22)$$

where A represents the scattering coefficient matrix, F is the discrete frequency distribution of the particle size, and G is the actual attenuation coefficient measured at a different frequency. The Equation 21 is a classical ill-posed problem and therefore the regularization factor γ and smoothing matrix H was introduced by (Jia et al (2019)) to solve the form of the matrix as follows.

$$F = (A^T A + \gamma H) A^T G \qquad (23)$$

The core matrix, A, is constructed as a 'forward problem' by summing the discrete particle size and frequencies. H is a smoothing matrix (a filter to reduce the noise), γ is the optimum factor (i.e., a Lagrange multiplier used to find local minimum and maximum values) (Su et al., (2008)). The solution of F represents a positive value for PSD.

In fluid-particle system the contribution of different particle size fractions to the overall ultrasound attenuations are linearly weighted with their concentration. The matrix of extinction coefficient A is given by:

$$A = \frac{4}{9}\sigma^4 + (\frac{\rho_p}{\rho_F} - 1)^2 - \frac{48{\varphi_r}^2(1+\varphi)\sigma}{81(1+\varphi_r)^2 + 16{\varphi_r}^4(\frac{\rho_p}{\rho_F} + \frac{1}{2} + \frac{9}{4\varphi_r})^2} \quad (24)$$

where, $\sigma = \frac{\pi d}{\lambda}, \varphi_r = \sqrt{\frac{\pi\rho_F f d^2}{4\eta_F}}$, d is particle diameter, λ is the wavelength, η_F is the dynamic fluid viscosity, f is transmitted wave frequency, ρ_p and ρ_F are particle and fluid viscosity, respectively. The optimal regularization technique (algorithm) was used by (Mingxu et al., (200)) by optimization of the γ factor to particle size distribution inversion. In Equation 23 F is a non-negative discrete frequency distribution of the particle size. To calculate the attenuation coefficient G_i in practice, two sensors are attached to the mixture wall in the opposite direction: one sensor sends the signal with a range of frequencies, and the other sensor receives the attenuated signal. The attenuation of the received signal can be calculated for each frequency by using Equation 2.

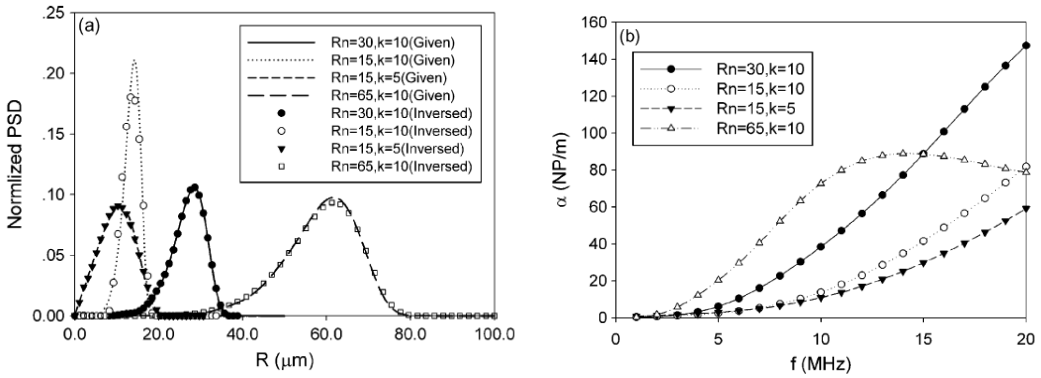

Figure 7: Numerical simulation employing *Optimum Regularization Technique* algorithm (a) inversed PSD; (b) predicted ultrasonic attenuation spectra expressed by Equation 17 (Rn is the characteristic radius parameter of Rosin-Rammer distribution and k is the uniformity coefficient) (Mingxu et al., (2008)).

Figure 7 shows a numerical solution following the above algorithm that was carried out for a glass beads aqueous suspension 1% (v/v) with the predicted attenuation spectra and PSD for different particle sizes (15, 30 and 65 μm) by (Mingxu et al., (2008)).

Richter et al., (2005)., also reported a methodology proposed by Faran (Faran, (1951))) to predict particle size distribution in a region of micro-sized particles using the measured attenuation spectrum. They first characterized particle volume fractions independently from the ultrasonic

attenuation with respect to particle size and shape. The results compared well against those from a commercial attenuation spectrometer.

3.3 Solid Volume Fraction

Ultrasound techniques can be used to measure the volume fraction of particles in dispersed fluid-particle flows. The dispersed phase volume fraction affects the ultrasound speed and the attenuation of the propagated wave (Poelma, (2020)). The ultrasound speed is dependent on the density and compressibility of the medium and is affected by the presence of solid particles and gas bubbles within the flow (Kong et al., (2017)). According to the literature in liquid-solid flows both the wave transmission time and the amplitude ratio (the ratio of the received signal amplitude, A_i, to the transmitted signal amplitude, A_o) decrease with increasing solid volume fraction (Soong et al., (1997), Jingyuan and Yong, (2016)). In addition, an increase in gas velocity increases the attenuation of the propagated wave. The change in ultrasound propagation speed and attenuation depends on the applied frequency, bubble, or particle size and on the dispersed phase volume fraction within a mixture (Tran et al., (2016), Wang et al., (2019)).

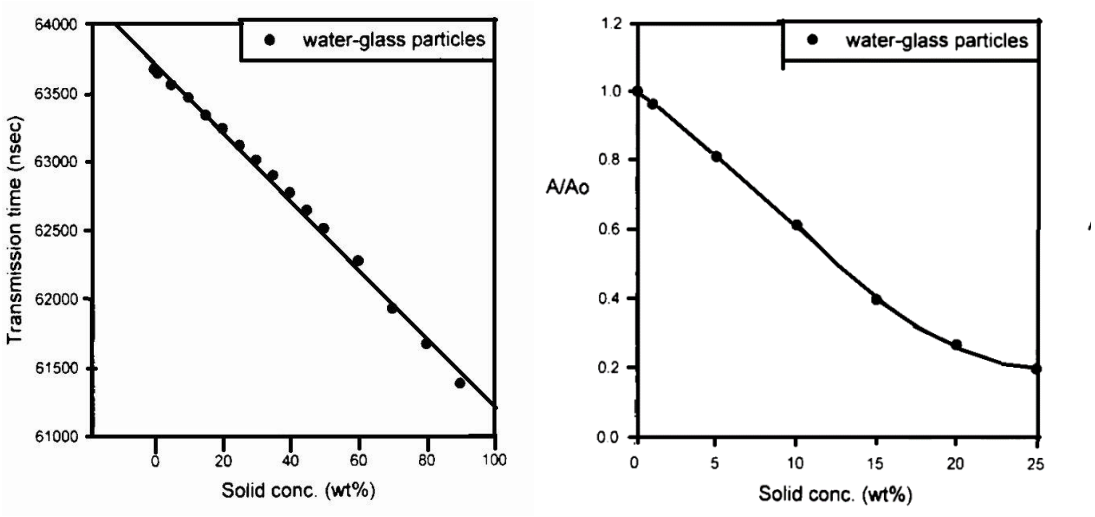

Figure 8: Transmission time and amplitude ratio vs solid concentration in a water-glass particle system measured at a frequency of 4 MHz (Stolojanu and Prakash, (1997)).

Figure 8 shows the transmission time and amplitude of the propagated ultrasound wave as a function of solid concentration in fluid (water)-particle flows within a Plexiglas channel with 0.1016 m diameter. Two ultrasonic sensors were used to generate and receive the signal through

the system. Excitation frequencies of 0.1 to 100 MHz were used to measure the transmission time of the ultrasound wave through a mixture of glass particles (35 μm) in water at a concentration of up to 90% by weight. For the amplitude measurements concentrations up to 25wt % were used (Stolojanu and Prakash, (1997)). As can be seen in Figure 8 both the transmission time and the amplitude ratio decrease with increasing particle concentration. The increase in gas velocity will increase the number of bubbles and this increases the transition time of the propagated wave (sound waves move slower in gas compared to liquid).

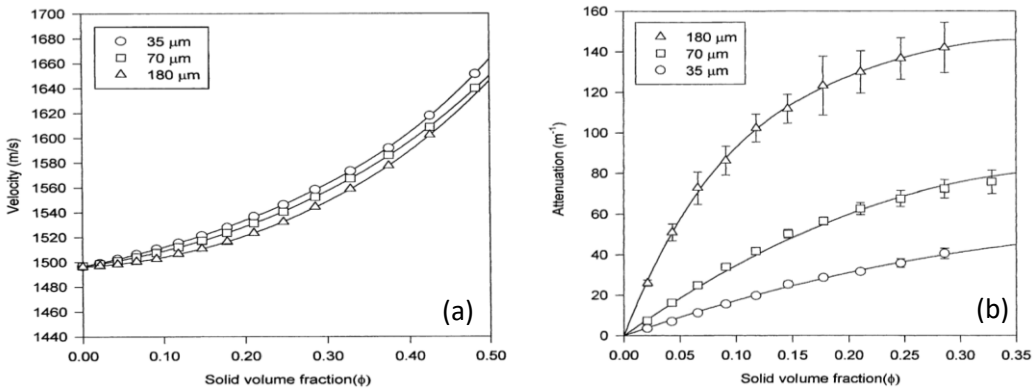

Figure 9: a) Variation of ultrasound velocity vs solid concentration and particle size in water-glass bead suspensions b) Attenuation as a function of solids volume fraction and particle size (Stolojanu and Prakash, (2001)).

In Figure 9 a, the results indicated that the acoustic wave speed decreases with increasing particle size. It is not clear what causes the change of velocity with increasing particle size. Figure 9 a also shows that the sound velocity increases with increasing solid particle volume fraction, which is expected because the sound speed increases with an in increase in both the compressibility and density of the medium. The effect of solid volume fraction (up to 45 vol%) of different particle sizes on ultrasound speed in slurry systems was reported by (Stolojanu and Prakash, (2001)) (Figure 9 b). To express the effect of solid volume fraction on attenuation, the following equation was proposed for the attenuation coefficient by (Stolojanu and Prakash, (2001)) :

$$\alpha = \sum_{i=1}^{n} \alpha_i = -\sum_{i=1}^{n} \frac{1}{x} ln\left(\frac{A_o}{A_i}\right) \qquad (25)$$

where, A_o is the initial amplitude, A_i is the attenuated amplitude and x is the distance the sound wave travels in the medium. Figure 9 b also shows that the attenuation increases with increasing particle size and solid volume fraction while the increase in volume fraction is more significant for the larger particle diameter.

An algorithm for determining the volume fraction of oil drops dispersed in a water continuous phase has been described by (Chaudhuri et al., (2012)). This analogous methodology could be used in other dispersed systems such as solid-liquid flows. Two models have been proposed to calculate the oil volume fraction, φ, by (Uric, (1947)) and (Atkinson and Wells, (1977)). The two models can be combined as follows. The volume fraction of oil in the mixture of oil V_o and water V_w is given by:

$$\varphi = (\frac{V_o}{V_o + V_w}) \tag{26}$$

From conservation of mass in an oil-water system.

$$\rho(V_o + V_w) = \rho_o V_o + \rho_w V_w \Rightarrow \rho = \rho_o \varphi + \rho_w (1 - \varphi) \tag{27}$$

where, ρ is the mixture density, ρ_o, ρ_w are the oil and water densities, respectively.

From the above equation:

$$\frac{\rho}{\rho_w} = \varphi \frac{\rho_o}{\rho_w} + (1 - \varphi) = 1 - \varphi(1 - r) \tag{28}$$

where $= \frac{\rho_o}{\rho_w}$. From Equation 27 and Equation 28 the following is found :

$$\frac{\rho}{\rho_w} = \frac{\rho_w(1 - \varphi) + \rho_o(2 + \varphi)}{\rho_w(1 + 2\varphi) + 2\rho_o(1 - \varphi)} = \frac{(1 - \varphi) + r(2 + \varphi)}{(1 + 2\varphi) + 2r(1 - \varphi)} \tag{29}$$

The speed of sound in oil, c_o, and in water, c_w, is expressed as:

$$c_o = \frac{1}{\sqrt{\kappa_o \rho_o}}, c_w = \frac{1}{\sqrt{\kappa_w \rho_w}} \tag{30}$$

where κ_o, κ_w are the oil and the water compressibility, respectively. Also:

$$\frac{\kappa_o}{\kappa_w} = \frac{\kappa_o}{\kappa_w}\frac{\rho_o}{\rho_w} \times \frac{\rho_w}{\rho_o} = \frac{{c_w}^2}{r{c_o}^2} = \frac{C_1}{rC_2} \tag{31}$$

Here $C_1 = \frac{c^2}{{c^2}_o}$, $C_2 = \frac{c^2}{{c^2}_w}$, c is the sound speed in the mixture, $c = 1/\sqrt{\rho\kappa}$, ρ is the density of the composite medium and κ is the adiabatic compressibility of the medium.

$$k = \varphi\kappa_o + (1 - \varphi)\kappa_w \tag{32}$$

From Equation 30 and Equation 31 it is found that:

$$\frac{\kappa}{\kappa_w} = \frac{\varphi\kappa_o}{\kappa_w} + (1 - \varphi) = 1 - \varphi(1 - \frac{C_1}{rC_2}) \tag{33}$$

By multiplying Equation 32 with Equation 23 the following quadratic Equation 28 is found:

$$A\varphi^2 + B\varphi + D = 0 \tag{34}$$

where $A = (C_1 - rC_2)(1 - r)$, $B = 2rC_2 - C_1 + r^2C_2 + 2r(1 - C_1 - r)$ and $D = r(1 + 2r)(1 - C_2)$.

The final solution of the quadratic equation is given as follows:

$$\varphi = \frac{-B \pm \sqrt{B^2 - 4AD}}{2A} \tag{35}$$

The solutions of Equation 35 are shown in Figure 10 for various temperatures, and this showed that the sound speed is a function of volume fraction and the density in water and crude oil. Chaudhuri et al., (2014) also reported the numerical study and reveals that, higher errors occur when the two-component fluids' properties (sound speed) are similar.

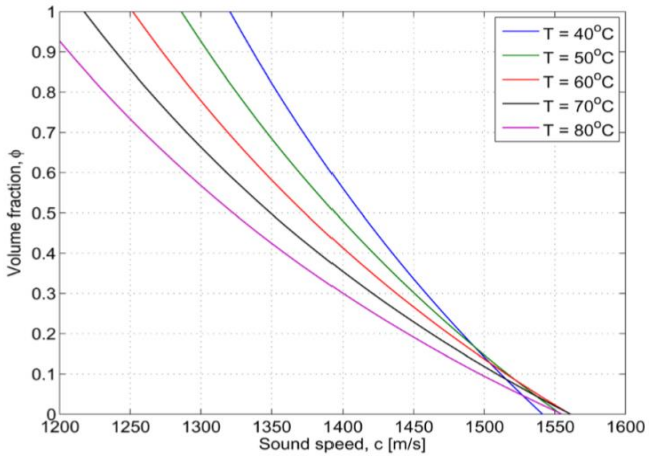

Figure 10: Volume fraction of crude oil in water as a function of the sound speed at different temperatures (Chaudhuri et al., (2014)).

4. Acoustic Emission AE Technique

The term acoustic emission (AE) describes both the phenomenon and the measurement technique. In fluid-particle systems the collision between particles or of the particles with the chamber wall releases energy in the form of elastic waves. The generation of the elastic waves is termed acoustic emission and depends on the nature of the sources. The elastic waves are generated in the range of ultrasound frequencies and can be detected via a microphone or a transducer (Scruby, (1987)). Acoustic emission elastic waves can also be generated when the internal structure of solid materials changes (Nsugbe et al., (2019)). The generated AE signals

are of practical interest in engineering for solids characterization in solid-gas flows, or for detection of leaks in flow systems. Here, in the following section 4.1, we introduced the application of acoustic emission technique to solid-gas flows.

4.1 Application of Acoustic Emission AE Technique to Solid-Gas Flows

Non-intrusive acoustic emission (AE) sensors can be applied to characterise the two-phase flow in solid-gas, solid-liquid and liquid-gas flows. The acoustic technique has not been applied to gas-liquid circulated fluidised beds. In gas-solid fluidised beds, an elastic wave may be generated from (1) particle-particle or particle-wall friction, (2) particle-particle or particle-wall collisions, and (3) air turbulence in the bed. This elastic wave includes both audible and high-frequency sound, which can be measured by the AE sensor. The acoustic wave of an AE transducer with a frequency of 40 kHz in the air is 0.01 dB, and this implies that the probe cannot reliably be used at a large distance from the source of elastic wave due to the high attenuation of the sound wave in the air. The AE sensors have a piezoelectric element which converts the mechanical sound wave into an electrical analogue signal, which is then amplified and converted to digital data and displayed on an oscilloscope. Xu et al., (2021) reported a series of experiments to measure the effect of the acoustic field on the fluidization characteristics of solid-gas separation fluidised bed. They concluded that the acoustic frequency changes with increasing the volume fraction of fine particles and sound pressure level, and the sound filed improves the efficiency of the contact between the air flow and the particles. Tsujimoto et al., (1999) developed a high-frequency 140 kHz AE sensor and applied it to a gas-solid fluidised bed. They reported the relationship between acoustic emission amplitude, gas velocity and dimensionless bed height. They used an acoustic sensor to measure the elastic wave of a sound generated by the fluidised particles in solid gas fluidised bed granulator. The generated elastic wave by friction and collisions of the fluidised particles propagated in all directions and collected by the AE sensor. The detected signal was amplified up to 40 dB. The output signal frequency was analysed using FFT. The AE signal filtered by the band pass filter to filter out the background noise. In general, the activity of the fluidised bed particles depends on the gas velocityU_s, beyond the minimum fluidisation velocity, U_{mf}. The frequency spectrum obtained from the fluidised bed particles at a gas phase velocity of U_s = 0.6 m/s is shown in Figure 11 a. The maximum AE amplitude recorded within the sensor frequency range of 125–375 kHz. The

change in both acoustic emission amplitude, A_{AE}, and the expanded bed height, H_f, are shown in Figure 11 b.

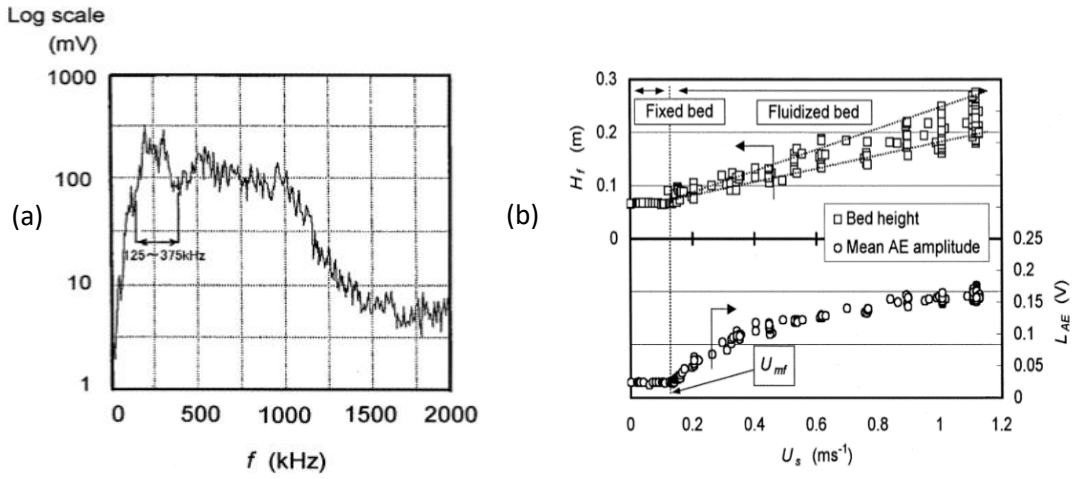

Figure 11: a) Frequency spectrum obtained from the fluidised bed particles at gas phase velocity of U = 0.6 m/s, and b) change in mean amplitude (L_{AE}) and fluidised bed height (H) with increasing fluidised bed gas velocity (U_s) (Tsujimoto et al., (1999)).

In Figure 11 b, the bed heights are also measured visually (dashed lines), while the square symbols indicate the bed height as measured by the acoustic emission sensor. An increase in the amplitude of the received signal with the gas phase velocity was related to the increase in the frequency and strength of particle-particle or particle-wall collisions beyond the minimum fluidisation velocity (0.128 m/s). The relationship between the measured AE amplitude and the gas velocity for various operating conditions is presented in Figure 12 a.

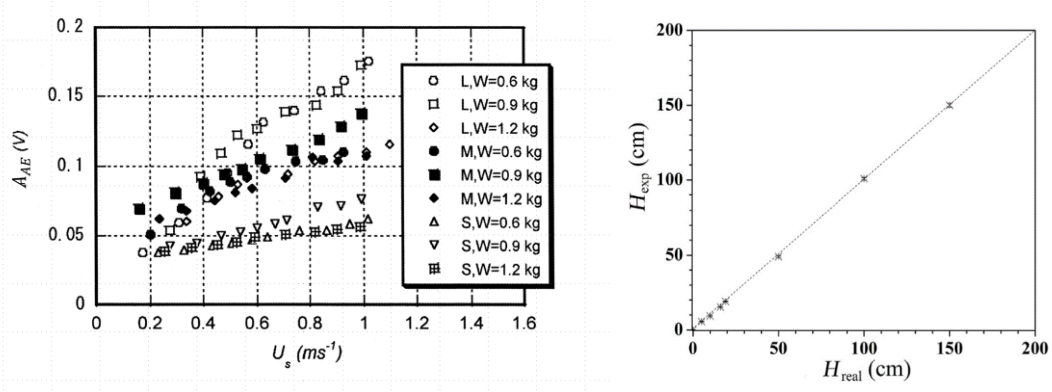

Figure 12: a) Effects of fluidised bed air velocity against mean AE amplitude at different size (L,M,S) and weight (W) of particles in a fluidised bed (Tsujimoto et al., (1999)), b) A comparison of ultrasound level measurements with visually measured bed levels in a hopper (H is the distance of the powder level from the probe) (Kong et al., (2017)).

The experimental conditions were fitted to the following equation:

$$A_{AE}(2.32 \times 10^{-4}/d)^{1.7} = 1.40 \times 10^{-2}\left[(U_s - U_{mf})/U_{mf}\right]^{0.40} \quad (36)$$

where d, denotes the particle diameter. For all sample sizes, small, medium, and large (S, M, L) in Figure 12 a, the AE amplitude increases with increasing gas velocity and particle size.

Briongos et al., (2005) showed that low-frequency acoustic emissions could be used to monitor solids in solid-gas fluidised beds. They developed a portable measurement system that is applicable to both laboratory and industrial scales. Jingdai et al. (2009) carried out acoustic emission measurements to monitor the patterns during particle fluidization. The results showed that the gas velocity, particle size, and static bed height significantly impacted the fluidization pattern.

Kong et al., (2017) also reported an acoustic displacement sensor (this sensor operates with a low frequency signal, $f = 40\,KHz$) monitoring technique for gas-solid fluidised beds, see Figure 12 b. The results from acoustic techniques were compared with data obtained from video-imaging. The bubble frequencies were found at 1.6, 1.8, and 1.9 1/sec, respectively, and these results were very close to the results obtained using video imaging (1.68, 1.82, and 1.88 s−1, respectively). Wang et al., (2019) investigated the detection of acoustic signals from the flow of sand in a steel pipeline. The AE signals were measured in two different positions (one at the upper surface of the pipe and the second after a bend). Sand particles with a diameter of 80 um, 96 um, 109 um, 125 um and 150 um and density of $2.65\ g/cm^3$ were mixed with water in the reservoir. They found that the AE [RMS] value is increasing with both the sand size and the concentration. The results indicated that the AE sensor could detect sand in water flow.

5. Conclusions

Ultrasound techniques were originally designed for medical imaging, but recent works have shown that they can be reliably used to study fluid-particle flows. Acoustic based measurements offer significant advantages over other techniques, such as fast response, real-time measurement, and possibility to use them with optically non-transparent test sections, often required for high pressure, high temperature processes or in reactors with radioactive content. In addition, acoustic equipment is cheap, not harmful and involves no radiation. Ultrasound techniques can be used in liquid-particle systems to obtain volume fraction of the particles, particle size distribution and velocity profiles. The main drawbacks of the ultrasound techniques are the relatively low spatial resolution and the maximum achievable frame rate. The use of high ultrasound frequencies can improve the time resolution, but can lead to high signal attenuation or reduced penetration depth. However, because of the large attenuation of sound in gases, ultrasound-based techniques cannot be used in gas-solid systems; in such system acoustic emission (AE) techniques are more appropriate. The main drawbacks associated with the acoustic emission AE techniques are low amplitude (which in noisy environments can make the discrimination of the signal difficult), the need for highly specialised sensors, the disturbances caused from high frequency signal sources such as turbulence, or possible interferences from nearby electromagnetic sources.

In summary, this paper showed that:

- The transit-time method can measure the average liquid velocities in single-phase flows. Methods based on the Doppler effect can measure particle, bubble/droplet, and liquid velocity profiles in fluid-particle systems.
- Ultrasound attenuation or sound speed measurements of a propagated sound wave in a fluid-particle mixture can be used to characterise volume fractions of particles or droplets in fluid-particle flows.
- Ultrasound attenuation techniques can be used to characterise particle size distribution in highly concentrated liquid-particle flows.
- The acoustic emission AE technique can be used to measure particle size and particle velocity in gas-particle flows.

Ultrasound techniques can be further applied to three phase flows, bubbly flows and liquid-liquid or liquid gas flows and to flow regime imaging. However, acoustic techniques require additional improvements in terms of building algorithms for data processing. Improvements can be achieved by employing machine learning to enhance the accuracy of flow measurements and to identify flow regimes by ultrasound. Machine learning has been used to improve the accuracy of real-time flow regime identification (Zhang et al., (2020)) and has recently emerged

as the leading learning tool in image analysis. The major performance improvements that can be achieved with machine learning greatly depend on the availability of large training datasets. However, the current availability of datasets in the application of fluid-particle flows is limited. Ultrasound and acoustic emission AE techniques that enable fast measurements are suitable for obtaining large number of data; their further development together with machine learning are therefore very promising.

This review demonstrated that acoustic-based methods (ultrasound and AE) can advance the fundamental understanding of fluid-particle flows and can help their monitoring and operation. Ultrasound and acoustic emission based measurements can be considered for many multiphase flow applications including fluid-bed systems, solid-liquid-gas systems in stirred vessels, and in small channels used for process intensification.

Acknowledgement: The authors would like to acknowledge the support from Engineering and Physical Sciences Research Council, UK, through the Programme Grant PREMIERE (EP/T000414/1).

Nomenclatures

Symbol	Abbreviations	Unit
A_{AE}	$Acoustic\ emission\ amplitude$	$mV\ or\ V$
A	$Wave\ amplitude$	$mV\ or\ V$
A_n	$Scattered\ wave\ amplitude$	$mV\ or\ V$
$\boldsymbol{c}$	$Sound\ Speed$	m/s
$\boldsymbol{x}$	$Distance$	$cm\ or\ m$
D	$Pipe\ diameter$	$cm\ or\ m$
f	$Frequency$	Hz
f_d	$Doppler\ frequency$	Hz
f_{prf}	$Pulse\ reputation\ frequency$	Hz
k	$Wave\ number$	cm^{-1}
κ	$Compressibility$	$m^{2/n}$
$\boldsymbol{t}$	$Time$	*sec*
U_{mf}	$Minimum\ fluidisation\ velocity$	*m/s*
U_s	$Gas\ phase\ velocity$	*m/s*
$V(x)$	$Particles\ velocity\ Profile$	*m/s*
Z	$Acoustic\ Impedance$	*Pa.s/m*
θ	$Wave\ transmission\ angle$	*Rad/m*
α	$Attenuation\ coefficient$	$cm^{-1} or\ m^{-1}$
ρ	$Density$	kg/m^3
R	$Reflection\ Coefficient$	…….

φ	$Volume\ fraction$	……..
ω	$Angular\ frequency$	*Rad/sec*
$\boldsymbol{r}$	$Particle\ radius$	*μm*
$\boldsymbol{t_n}$	$Delay\ time$	*sec*
$\boldsymbol{\gamma}$	$Optimum\ factor$	……
λ	$Wave\ length$	*m*
η_F	$Fluid\ viscosity$	*Pa.sec*

References

AFANEH, A., ALZEBDA, S., IVCHENKO, V. & KALASHINKOV, N. (2011). Ultrasonic measurements of temperature in aqueous solutions: Why and how. Physics Research International, 2011**,** 1-10.

ALLEGRA, J. R. & HAWLEY, S. A. (1972). Attenuation of sound in suspensions and emulsions: Theory and experiments. J. Acoust. Soc. Am, 51**,** 1545-1564.

ARITOMI, M., KIKURA, H. & SUZUKI, Y. (2000). Ultrasonic Doppler method for bubbly flow measurement. Ohokayama, Meguro-Ku, Tokyo 152**,** 1-20.

ATKINSON, C. M. & KYTO¨MAA, H. K. (1993). Acoustic properties of solid-liquid mixtures and the limits of ultrasound diagnostics—i: Experiments (data bank contribution. Journal Of Fluids Engineering, 115**,** 665-675.

ATKINSON, P. & WELLS, P. N. (1977). Pulse-doppler ultrasound and its clinical application. Yale J Biol Med, 50**,** 367-73.

BAKER, J. P. (2005). The history of sonographers. J Ultrasound Med, 24**,** 1-14.

BOHS, L. N., GEIMAN, B. J., ANDERSON, M. E., GEBHART, S. C. & TRAHEY, G. E. (2000). Speckle tracking for multi-dimensional flow estimation. Ultrasonics, 38**,** 369-75.

BOUSSEL, L., RAYZ, V., MARTIN, A., ACEVEDO-BOLTON, G., LAWTON, M. T., HIGASHIDA, R., SMITH, W. S., YOUNG, W. L. & SALONER, D. (2009). Phase-contrast magnetic resonance imaging measurements in intracranial aneurysms in vivo of flow patterns, velocity fields, and wall shear stress: Comparison with computational fluid dynamics. Magn Reson Med, 61**,** 409-17.

BOYD, J. W. R. & VARLEY, J. (2001). The use of passive measurement of acoustic emission from chemial engineering process. Chem Eng Sci, 56**,** 1749-1756.

CARD, D. C., SIMS, G. E. & CHANT, R. E. (1971). Ultrasonic velocity of sound and void fraction in a bubbly mixture. J. Basic Engn.Q., **,** 619-623.

CENTS, A. H. G., BRILMAN, D. W. F. & VERSTEEG, G. F. (2004). Measuring bubble, drop and particle sizes in multiphase systems with ultrasound. Wiley Interscience, 50**,** 11.

CHAUDHURI, A., OSTERHOUDT, C. F. & SINHA, D. N. (2012). An Algorithm for Determining Volume Fractions in Two-Phase Liquid Flows by Measuring Sound Speed. Journal of Fluids Engineering, 134**,** 101301-1.

CHAUDHURI, A., SINHA, D. N., ZALTE, A., PEREYRA, A., WEBB, C. & GONZALEZ, M. E. (2014). Mass Fraction Measurements in Controlled Oil-Water Flows Using Noninvasive Ultrasonic Sensors. Journal of Fluids Engineering, 136**,** 031304-1.

CHIRONE, R., RAGANATI, F., AMMENDOLA, P., BARLETTA, D., LETTIERI, P. & POLETTO, M. (2018). A comparison between interparticle forces estimated with direct powder shear testing and with sound assisted fluidization. Powder Technology, 323**,** 1-7.

CHUN, S., YOON, B. & LEE, K. B. (2011). Diagnostic flow metering using ultrasound tomography. Journal of Mechanical Science and Technology, 25**,** 1475-1482.

CONRAD, K. & LYNNWORTH, L. (2002). Fundamentals of ultrasonic flow meters. American School Of Gas Measurement Technology.

DE-LA-CRUZ-TORRES, B., BARRERA-GARCIA-MARTIN, I., ALMAZAN-POLO, J., JAEN-CRESPO, G. & ROMERO-MORALES, C. (2020). Ultrasound imaging evaluation of structural and textural features in asymptomatic achilles tendons in pre-professional dancers: A cross-sectional study. Physical Therapy in Sport, 44**,** 85-91.

DOSRAMOS, J. G. (2012). Acoustic attenuation spectroscopy for process control of dispersed systems. Materials Science and Engineering, 42**,** 012023.

DE-LA-CRUZ-TORRES, B., BARRERA-GARCIA-MARTIN, I., ALMAZAN-POLO, J., JAEN-CRESPO, G. & ROMERO-MORALES, C. (2020). Ultrasound imaging evaluation of structural and textural features in asymptomatic achilles tendons in pre-professional dancers: A cross-sectional study. Physical Therapy in Sport, 44**,** 85-91.

EPSTEIN, P. S. & CARHART, R. R. (1953). The absorption of sound in suspensions and emulsions. I. Water fog in air. The Journal of the Acoustical Society of America, 25.

EREN, H. (1998). Accuracy in Real Time Ultrasonic Applications and 'Transit-Time Flow Meters. IEEE Instrumentation and Measurement 18**,** 586-572.

FARAGE, H., MEJDELL, T., HJARBO, K., EGE, P., LYSBERG, M., GRISLINGAS, A. & DE LASA, H. (1997). Fibre optic and capacitance probes in turbulent fluidized beds. Chemical Engineering Communication, 157**,** 73-107.

FARAN, J. J. (1951). Sound Scattering by Solid Cylinders and Spheres. The Journal of the Acoustical Society of America, 23**,** 405-418.

FLORES, N., KURI-MORALES, Á. & GAMIO, C. An Application of Neural Networks for Image Reconstruction in Electrical Capacitance Tomography Applied to Oil Industry. In: MARTÍNEZ-TRINIDAD, J. F., CARRASCO OCHOA, J. A. & KITTLER, J., eds. Progress in Pattern Recognition, Image Analysis and Applications, 2006// (2006) Berlin, Heidelberg. Springer Berlin Heidelberg, 371-380.

GLADDEN, L. F. (2003). Recent Advances in MRI Studies of Chemical Reactors: Ultrafast Imaging of Multiphase Flows. Topics in Catalysis, 24**,** 19-28.

HALLS, B. R., RAHMAN, N., MEYER, T. R., LIGHTFOOT, M. D. A., SLIPCHENKO, M. N., ROY, S. & GORD, J. R. Four-Dimensional X-ray Imaging of Multiphase Flows. Imaging and Applied Optics 2018/06/25 (2018) Orlando, Florida. Optical Society of America, LM3C.2.

HAN-LIANG, X. & LING-AN, X. (2000). Electromagnetic tomography (EMT): Theoretical analysis of the forward problem. Applied Mathematics and Mechanics, 21**,** 1034-1044.

HAN, E., VAN HA, N. & JAEGER, H. M. (2017). Measuring the porosity and compressibility of liquid-suspended porous particles using ultrasound. Soft Matter, 13**,** 3506-3513.

HIROSHIGE, K., HIDEKI, M. & MASANORI, A. (2009). Velocity profile measurements in bubbly flow using multi-wave ultrasound technique. Chemical Engineering Communications, 197**,** 114-133.

HOSSEIN, F. (2019). Colloid Vibration Potential for Imaging in Engineering and Medicine. Ph.D, University of Leeds.

HOSSEIN, F. & WANG, M. (2019). Colloid vibration potential imaging for medicine. J Biomed Imag Bioeng, 3**,** 114-118.

HOSSEIN, F. & WANG, M. (2020). Modelling and measurement of ultrasound vibration potential distribution in an agar phantom. Chemical Physics, 534**,** 110757.

HUNTER, T. N., PEAKALL, J. & BIGGS, S. R. (2011). Ultrasonic velocimetry for the in situ characterisation of particulate settling and sedimentation. Minerals Engineering, 24**,** 416-423.

ISMAIL, I., GAMIO, J. C., BUKHARI, S. F. A. & YANG, W. Q. (2005). Tomography for multi-phase flow measurement in the oil industry. Flow Measurement and Instrumentation, 16**,** 145-155.

JINGYUAN, S. & YONG, Y. (2016). Non-intrusive measurement and hydrodynamics characterization of gas–solid fluidized beds: a review. Meas. Sci. Technol, 27**,** 112001.

KIKURA, H., MURAKAWA, H. & ARITOMI, M. (2009). Velocity profile measurements in bubbly flow using multi-wave ultrasound technique. Chemical Engineering Communications, 197**,** 114-133.

KLINZING, G. E., RIZK, F., MARCUS, R. & LEUNG, L. (2011). Pneumatic conveying of solids: a theoretical and practical approach, Springer Science & Business Media.

KONG, W., LI, S., KE, H., ZHANG, H. & BAEYENS, J. (2017). The use of ultrasound probes to monitor multi-phase behaiviour in opaque systems. Particuology, 45**,** 91-97.

LAURENT, A., SEBASTIEN, M. & MATHIAS, F. (2001). Ultrafast two dimensional ultrasonic speckle velocimetry: A tool in flow Imaging. Applied Physics Letter, 78**,** 155-1158.

LEI, J. & LIU, S. (2011). An Image Reconstruction Algorithm Based on the Regularized Minimax Estimation for Electrical Capacitance Tomography. Journal of Mathematical Imaging and Vision, 39**,** 269-291.

LI, X., JAWORSKI, A. J. & MAO, X. (2018). Comparative study of two non-intrusive measurement methods for bubbling gas-solids fluidized beds: Electrical capacitance tomography and pressure fluctuations. Flow Measurement and Instrumentation, 62**,** 255-268.

MAAß, S., WOLLNY, S., VOIGT, A. & KRAUME, M. (2011). Experimental comparison of measurement techniques for drop size distributions in liquid/liquid dispersions. Experiments in Fluids, 50**,** 259-269.

MACRÌ, D., SUTCLIFFE, S. & LETTIERI, P. (2020). Fluidized bed sintering in TiO2 and coke systems. Chemical Engineering Journal, 381**,** 122711.

MEDWIN, H. (1976). Counting bubble accoustically: a review. Ultrasonics - Sonochemistry**,** 7-13.

MERIBOUT, M., SHEHZAD, F., KHAROUA, N. & KHEZZAR, L. (2020). An ultrasonic-based multiphase flow composition meter. Measurement, 161**,** 107806.

MINGXU, S., MINGHUA, X., XIAOSHU, C., ZHITAO, S. & FENG, X. (2008). Particle size chracterisation by ultrasonic attenuation spectra. Particulogy, 6**,** 276-281.

MORI, M., TAKEDA, Y., TAISHI, T., FURUICHI, N., ARITOMI, M. & KIKURA, H. (2002). Development of a novel flow metering system using ultrasonic velocity profile measurement Experiments in Fluids, 32**,** 153-160.

MOUGINA, P., WILKINSONA, D., ROBERTSB, K., J., JACKC, R. & KIPPAX, P. (2003). Sensitivity of particle sizing by ultrasonic attenuation spectroscopy to material properties. Powder Technology, 134**,** 243-248.

MUÑOZ-COBO, J. L., CHIVA, S., MÉNDEZ, S., MONRÓS, G., ESCRIVÁ, A. & CUADROS, A. J. L. (2017). Sensitivity of particle sizing by ultrasonic attenuation spectroscopy to material properties. . Powder Technology, 134**,** 243-248.

NAN, J., MING-XU, S. & XIAO-SHU, C. (2019). Particle size distribution measurement based on ultrasonic attenuation spectra using burst superposed wave. Results in Physic, 13**,** 102273.

NGAN, K. H., IOANNOU, K., RHYNE, L. D., WANG, W. & ANGELI, P. (2009). A methodology for predicting phase inversion during liquid–liquid dispersed pipeline flow. Chemical Engineering Research and Design, 87**,** 318-324.

NGUYEN, T. H. L. & PARK, S. (2019). Multi-Angle Liquid Flow Measurement Using Ultrasonic Linear Array Transducer. Sensors, 20**,** 1-13.

NSUGBE, E., STARR, A., JENNIONS, I. & RUIZ-CARCEL, C. (2019). Estimation of online particle size distribution of a particle mixture in free fall with acoustic emission. *Particulate Science and Technology,* 37**,** 953-963.

ÖRLÜ, R. & ALFREDSSON, P. H. (2010). On spatial resolution issues related to time-averaged quantities using hot-wire anemometry. Experiments in Fluids, 49**,** 101-110.

ORTIZ, S. H. C., CHIU, T. & FOX, M. D. (2012). Ultrasound image enhancement: A review. Biomedical Signal Processing and Control, 7**,** 419-428.

PARKER, D. J. & FAN, X. (2008). Positron emission particle tracking—Application and labelling techniques. Particuology, 6**,** 16-23.

PATRICIA, M. & DEREK, W. (2000). Characterization of particle size and its distribution during the crystallization of organic fine chemical products as measured in situ using ultrasonic attenuation spectroscopy. Acoustical Society of America, 109**,** 274-282.

PIRRI, C., STECCO, A., FEDE, C., DE CARO, R., STECCO, C. & OZCAKAR, L. (2020). Ultrasound imaging of a scar on the knee: Sonopalpation for fascia and subcutaneous tissues. Eur J Transl Myol, 30**,** 8909.

POELMA, C. (2017). ultrasound imaging velocimetry: a review. Exp Fluids, 58**,** 1-28.

POELMA, C. (2020). Measurement in opaque flows: a review of measurement techniques for dispersed multiphase flows. Acta Mech, 231**,** 2089-2111.

POELMA, C., WESTERWEEL, J. & OOMS, G. (2006). Turbulence statistics from optical whole-field measurements in particle-laden turbulence. Exp Fluids 40(3):347–363.

PORE, M., ONG, G. H., BOYCE, C. M., MATERAZZI, M., GARGIULI, J., LEADBEATER, T., SEDERMAN, A. J., DENNIS, J. S., HOLLAND, D. J. & INGRAM, A. J. (2015). A comparison of magnetic resonance, X-ray and positron emission particle tracking measurements of a single jet of gas entering a bed of particles. Chemical Engineering Science, 122**,** 210-218.

RAMSKILL, N. P., SEDERMAN, A. J., MANTLE, M. D., APPEL, M., DE JONG, H. & GLADDEN, L. F. (2018). In Situ Chemically-Selective Monitoring of Multiphase Displacement Processes in a Carbonate Rock Using 3D Magnetic Resonance Imaging. Transport in Porous Media, 121**,** 15-35.

RAINE, A. B., ASLAM, N., UNDERWOOD, C. P. & DANAHER, S. (2015). Development of an ultrasonic airflow measurement device for ducted air. Sensors (Basel), 15**,** 10705-22.

RICHTER, A., BABICK, F. & RIPPERGER, S. (2005). Polydisperse particle size characterization by ultrasonic attenuation spectroscopy for systems of diverse acoustic contrast in the large particle limit. The Journal of the Acoustical Society of America, , 118**,** 1394-1405.

RIEBEL, U. & LOFFLER, F. (1989). The fundamentals of particle size analysis by means of ultrasonic spectrometry. Particle and Particle System Characterization, 6**,** 136-143.

ROJAS, G. & LOEWEN, M. R. (2007). Fiber-optic probe measurements of void fraction and bubble size distributions beneath breaking waves. Experiments in Fluids, 43**,** 895-906.

SARI, D., VUARNOZ, F. & MEIL, J. (2000). Visualization of ice slurries and ice slurry flows Second Workshop on Ice Slurries of the International Institute of Refrigeration 22**,** 68-81.

SAVINO, K. & AMBROSIO, G. (2019). Handheld ultrasound and focused cardiovascular echography: Use and information. Medicina (Kaunas), 55.

SCRUBY, C. B. (1987). An introduction to acoustic emission. *Journal of Physics E: Scientific Instruments,* 20**,** 946-953.

SERIZAWA, A., KATAOKA, I., GOFUKU, A., TAKAHASHI, O. & KAWARA, Z. (1991). In: Proceedings of the International Conference on Multiphase Flows'. Tsukuba, Japan, **,** 547–550.

SIGEL, B. (1998). A brief history of Doppler ultrasound in the diagnosis of peripheral vascular disease. Ultrasound Med Biol, 24**,** 169-76.

SOONG, Y., ISAAC, K., GAMWO, F. W., HARKE, A. G., BLACKWELL, R., SCHEHL, R. & MICHAEL F. Z. (1997). Measurement of solids concentration by an ultrasonic transmission technique. Chem. Eng. Technol, 20**,** 47-52.

SPELT, P. D. M., MICHAEL, A., NORATO, A., ASHOK, S., SANGANI, S. & TAVLARIDES, L. L. (1999). Determination of particle size distributions from acoustic wave propagation measurements. Physics of Fluids, 11**,** 1065-1080.

SPINELLI, E., MAURI, T., FOGAGNOLO, A., SCARAMUZZO, G., RUNDO, A., GRIECO, D. L., GRASSELLI, G., VOLTA, C. A. & SPADARO, S. (2019). Electrical impedance tomography in perioperative medicine: careful respiratory monitoring for tailored interventions. BMC Anesthesiology, 19**,** 140.

STAKUTIS, V. J., MORSE, R. W., DILL, M. & BEYER, R. T. (1955). Attenuation of Ultrasound in Aqueous Suspensions. The Journal of the Acoustical Society of America, 27**,** 3539-546.

STOLOJANU, V. & PRAKASH, A. (1997). Hydrodynamic measurements in a slurry bubble column using ultrasonic techniques. Chemical Engineering Science, 52**,** 4225-4230.

STOLOJANU, V. & PRAKASH, A. (2001). Characterization of slurry systems by ultrasonic techniques Chemical Engineering Journal 84**,** 2015-2022.

SU, M., XU, F., CAI, X., REN, K. & SHEN, J. (2007). Optimization of regularization parameter of inversion in particle sizing using light extinction method. China Particuology, 5**,** 295-299.

SU, M., XUE, M., CAI, X., SHANG, Z. & XIU, F. (2008). Particle size characterization by ultrasonic attenuation spectra. Particuology, 6**,** 276-281.

TAKEDA, Y. (1986). Velocity profile measurement by ultrasound Doppler shift method. International Journal of Heat and Fluid Flow, 7**,** 313-318.

TAKEDA. Y. (2013). Instantanious velocity profile measurement by ultrasounic Doppler method. JSME International Journal, 38**,** 1995.

THAO, N., DAISUKE, S., TOMOHISA, N., HIDEYUKI, N. & QUI TRAN-CONG. M. (2016). Determination of particle size distribution and elastic properties of silica microcapsules by ultrasound spectroscopy. Japanese Journal of Applied Physics 55**,** 07KC01.

THI, H., LY, N. & SUHYUN, P. (2020). Multi-angle liquid flow measurement using ultrasonic linear array transducer. Sensors, 20**,** 1-13.

THONG-UN, N., WONGSAROJ, W., TREENUSON, W., CHANWUTITUM, J. & KIKURA, H. (2018). An experimental study of different signal processing methods on ultrasonic velocity profiles in a single phase flow. Engineering Journal, 22**,** 124-141.

THONG-UN, N., WONGSAROJ, W., TREENUSON, W., CHANWUTITUM, J. & KIKURA, H. J. E. J. 2018. An Experimental Study of Different Signal Processing Methods on Ultrasonic Velocity Profiles in a Single Phase Flow. 22**,** 123-142.

TOMONORI, I., HIROSHIGE, K. & YASUSHI, T. (2013). Ultrasonic velocity profiler for very low velocity field. Flow Measurement and Instrumentation's, 34**,** 127-133.

TRAN, T. N., SHIBATA, D., NORISUYE, T., NAKANISHI, H. & MIYATA, Q. T. (2016). Determination of particle size distribution and elastic properties of silica microcapsules by ultrasound spectroscopy. Japanese Journal of Applied Physics, 55**,** 07KC01.

TSUJIMOTO, H., YOKOYAMA, T., HUANG, C. C. & SEKIGUCHI, I. (1999). Monitoring particle fluidization in a fluidized bed granulator with an acoustic emission sensor. Powder Technology 113**,** 88-96.

UHER, M. & BENEŠ, P. Measurement of particle size distribution by the use of acoustic emission method. 2012 IEEE International Instrumentation and Measurement Technology Conference Proceedings, 13-16 May 2012 (2012). 1194-1198.

URIC, R. J. (1947). A Sound Velocity Method for Determining the Compressibility of Finely Divided Substances. Journal of Applied Physics, 18**,** 983-987.

VATANAKUL, M., ZHENG, Y. & COUTURIER, M. (2004). Application of Ultrasonic Technique in Multiphase Flows. Ind. Eng. Chem. Res, 43**,** 5681-5691.

VOULGAROPOULOS, V. & ANGELI, P. (2017). Optical measurements in evolving dispersed pipe flows. Experiments in Fluids, 58**,** 1-15.

WANG, C., CONNOLLEY, T., TZANAKIS, L., ESKIN, D. & MI, J. (2019). Characterization of ultrasonic bubble clouds in a liquid metal by synchrotron x-ray high speed imaging and statistical analysis. Materials 13**,** 44.

WANG, G. & CHING, C. Y. (2001). Measurement of multiple gas-bubble velocities in gas–liquid flows using hot-film anemometry. Experiments in Fluids, 31**,** 428-439.

WANG, K., LIU, G., LI, Y., WANG, J., WANG, G., QIN, M. & YI, L. 2019. An investigation of the detection of acoustic sand signals from the flow of solid particles in pipelines. Chemical engineering research & design, 144**,** 272-284.

WANG, T., WANG, J., REN, F. & JIN, Y. (2002). Application of Doppler ultrasound velocimetry in multiphase flow. Chemical Engineering Journal 92**,** 111-122.

WEILING, L., CHAO, T. & FENG, D. (2018). Oil-water two-phase flow velocity measurement with continuous wave ultrasonic Doppler. Journal of Physics**,** 092019.

WELLS, P. N. (1975). Ultrasonic diagnostics: a look into the future. Biomed Eng, 10**,** 247-51.

WERTHER, J. (1992). Scale-up modeling for fluidized bed reactors. Chemical Engineering Science, 47**,** 2457-2462.

WINDOWS-YULE, C. R. K., SEVILLE, J. P. K., INGRAM, A. & PARKER, D. J. (2020). Positron Emission Particle Tracking of Granular Flows. Annual Review of Chemical and Biomolecular Engineering, 11**,** 367-396.

WÖCKEL, S., HEMPEL, U., WESER, R., WESSELY, B. & AUGE, J. (2012). Particle characterization in highly concentrated suspensions by ultrasound scattering method. Procedia Engineering, 47**,** 582-585.

WONGSAROJ, W., HAMDANI, A., TAISHI, T., TAKAHASHI, T. & KIKURA, H. (2018). Ultrasonic Measurement of Velocity Profile on Bubbly Flow Using a Single Resonant Frequency. Proceedings, 2**,** 1-7.

WU, W. T., CHANG, K. V. & OZCAKAR, L. (2020). Ultrasound Imaging and Guided Hydrodissection in the Management of a Postamputation Deep Peroneal Neuroma. Pain Pract**,** 695-696.

XIAOXIAO, D., CHAO, T., YE, Y. & FENG, D. (2015). Oil–water two-phase flow velocity measurement with continuous wave ultrasound Doppler. Chemical Engineering Science, 135**,** 155-165.

XU, X., FU, Y., SONG, S., DONG, L., LV, B., CHEN, Z., TIAN, Y. & CHEN, J. (2021). Fluidization and separation characteristics of a gas–solid separation fluidized bed in the presence of an acoustic field. Chemical Engineering Research and Design, 169**,** 46-53.

YAN, L., MIAO, W. & LI, D. (2020). Ultrasound imaging based on magnetic lipid microbubble contrast agent with fe(3)o(4) nanoparticles. J Nanosci Nanotechnol, 20**,** 6087-6093.

YANG, Z. & JOHNSON, M. (2017). Hybrid particle image velocimetry with the combination of cross-correlation and optical flow method. Journal of Visualization, 20**,** 625-638.

YATES, J. G. & LETTIERI, P. (2016). Fluidized-bed reactors: processes and operating conditions, Springer.

YEE, M. Q. Y., YEOW, B. S. & REN, H. (2019). Dispersion characterization of magnetic actuated needleless injections with particle image velocimetry. Medical & Biological Engineering & Computing, 57**,** 2435-2447.

ZHANG, Y. Q., WEN, J. X., LUO, R. K., YUAN, H. X. & WANG, W. P. (2020). Imaging and contrast-enhanced ultrasound features of duodenal neuroendocrine tumor: A case report. Clin Hemorheol Microcirc, 76**,** 27-32.

ZHOU, B., FRASER, K. H., POELMA, C., MARI, J. M., ECKERSLEY, R. J., WEINBERG, P. D. & TANG, M. X. (2013). Ultrasound imaging velocimetry: effect of beam sweeping on velocity estimation. Ultrasound Med Biol, 39**,** 1672-81.

(2008). Thermocouples. In: LI, D. (ed.) Encyclopedia of Microfluidics and Nanofluidics. Boston, MA: Springer US.